Supporting Information

Isomerization of second generation isoprene peroxy radicals: epoxide formation and implications for secondary organic aerosol yields

Emma L. D'Ambro[1,2], Kristian H. Møller[3], Felipe D. Lopez-Hilfiker[1,a] , Siegfried Schobesberger[1,b] , Jiumeng Liu[4], John E. Shilling[4,5], Ben Hwan Lee[1], Henrik G. Kjaergaard[3], Joel A. Thornton[*,1,2]

[1]Department of Atmospheric Sciences, University of Washington, Seattle, Washington 98195, United States
[2]Department of Chemistry, University of Washington, Seattle, Washington 98195, United States
[3]Department of Chemistry, University of Copenhagen, Universitetsparken 5, DK-2100 Copenhagen Ø, Denmark
[4]Atmospheric Sciences and Global Change Division, Pacific Northwest National Laboratory, Richland, WA, 99352, USA
[5]Environmental Molecular Sciences Laboratory, Pacific Northwest National Laboratory, Richland, WA, 99352, USA
[a]Now at: Laboratory of Atmospheric Chemistry, Paul Scherrer Institute, Zurich, Switzerland
[b]Now at: Department of Applied Physics, University of Eastern Finland, Kuopio, Finland

Author Information
Corresponding Author
[*]Phone: 206-543-4010; Email: thornton@atmos.uw.edu; Mail: 408 ATG Building, Box 351640, University of Washington, Seattle, WA 98195

This file includes:

Chamber conditions

The input isoprene concentration, 20 ppbv, is the concentration achieved in the chamber at steady state in the absence of any radical chemistry (i.e. UV-VIS lights off) while all else such as chamber residence time remained the same. A calibrated cylinder of isoprene (Matheson, 20 ppm isoprene in nitrogen) and a mass flow controller maintained steady delivery over the course of the experiments. H_2O_2 (Sigma-Aldrich, 50% in water) was introduced into the chamber via an automated syringe operated at various flow rates to achieve approximately 0.5, 2, 5, and 10 ppm input H_2O_2 concentrations (lights off). The delivery is less precise at lower flow rates. Therefore we used the H_2O_2 signal measured by the HRToF-CIMS to correct the H_2O_2 concentration at low injection rates assuming the values for 2, 5, and 10 ppm were correct. The ratio of HRToF-CIMS signal to the input concentration was the same to within 17% for the three highest H_2O_2 concentrations, but diverged significantly for the lowest desired H_2O_2 input, which, after correcting by the measured HRToF-CIMS signal was found to be 0.15 ppm.

0-D Chemical Kinetics Model

The Framework for 0-D Atmospheric Modeling (F0AM)[1] is a zero dimensional, i.e. single box, chemical kinetics model developed from the CAFE model[2-4] that incorporates the Master Chemical Mechanism (v3.3.1) from the University of Leeds.[5] This model, predominantly as its CAFE version, has been used extensively to analyze ground-based,[1, 3, 4, 6-10] aircraft-based,[1, 11-16] and ship-based[17] atmospheric data, as well as chamber data.[18, 19] We utilized the isoprene scheme in the MCM, although we added our own customized mechanism as mentioned in the main text to include the formation of $C_5H_{12}O_6$ and related compounds from this pathway. The hydroxy dihydroperoxy aldehyde, hydroxy dihydroperoxy ketone, and dihydroxy hydroperoxy epoxide were added as products of the isomerization of $C_5H_{11}O_6$• (Scheme 2) at relative yields of 0.5, 0.5, and 99%, and assigned c* of 20, 0.2, and 40 μg m^{-3}, respectively. A loss reaction for the dihydroxy hydroperoxy epoxide with OH was added in the gas-phase with an estimated rate constant of 5×10^{-11} s^{-1}, consistent with similar OH reactions in the MCM. New compounds as part of this mechanism and not in the current MCM version are shown in Table S1 with their molecular formula, SMILE string, structure, and a unique abbreviation. We have also made more minor adjustments. For example, the MCM includes OH oxidation of ISOPOH ($C_5H_{10}O_2$) to an alkoxy radical ($C_5H_9O_2$•) or fragments (methyl vinyl ketone +formic acid) depending on the isomer, rather than OH addition to the remaining double bond. We replace this reaction of OH + ISOPOH with two reactions: one that produces the alkoxy radical or fragments at 10% yield, as well as the same reaction that yields peroxy radicals at 90% yield, all at the original rate specified by the MCM. We also replace the IEPOX formation reactions in order to manipulate the yields between ISOPOOH + OH to IEPOX versus $C_5H_{11}O_6$• peroxy radical.

The added reactions and rate constants are shown in SI Table 2 utilizing the abbreviations for compounds. Abbreviations that are not specified in SI Table 2 are already in the MCM mechanism available online. Reaction rate constants are taken from similar reactions or literature values, and where possible we use MCM defaults. Defaults

are as follows: J41 (organic peroxide photolysis) = 5.787×10^{-6} s^{-1}, KRO2NO (RO_2+NO) = $2.7\times10^{-12}\times\exp(360/T)$ s^{-1}, KRO2HO2 (RO_2+HO_2) = $2.91\times10^{-13}\times\exp(1300/T)$ s^{-1}, KRO2NO3 (RO_2+NO_3) = 2.3×10^{-12} s^{-1}, KDEC (decomposition of an alkoxy radical) = 1×10^{6} s^{-1} where T is temperature in kelvin. Some reactions have been incorporated into the code but are currently given a rate coefficient of zero.

The set of 2,090 gas-phase reactions involving 645 species, including dynamic condensation and evaporation of 101 of those species to an organic phase leads to a fairly stiff set of differential equations. Matlab's ODE15s differential equation solver was used with a dynamic time-step approach, which we called repeatedly to solve 100 s integration segments. Concentrations predicted at the end of a 100 s integration segment are utilized as the inputs to the next 100 s segment.

The model was initialized with input concentrations of isoprene and H_2O_2 (see Table S3) and run for a total integration time of 2 days for each experimental condition which allowed for the model to reach chemical steady state, i.e. production and loss of species were equal and thus concentrations were unchanging. A chamber dilution rate of 5.6×10^{-5} s^{-1} was applied to all species based on the chamber flow conditions (35 L min^{-1}). Photolysis frequencies (J_x) were adjusted to account for the chamber lamp spectra. The NO_2 J-value was fixed to 0.006 s^{-1} as measured in the chamber. $J_{H_2O_2}$ was found to be 2.5×10^{-6} s^{-1} by modeling the isoprene decay rate from the time of lights on (Fig. SI 1). Seed particles are initialized at the beginning of each run (10^4 cm^{-3} with a radius of 25×10^{-7} cm), along with a small amount (0.002 μg m^{-3}) of existing organic aerosol phase to allow the partitioning of low volatility products to begin without explicitly modeling the nucleation of an organic phase. The volume and surface area of the modeled SOA are dynamically calculated at each 100 s integration segment by calculating the total mass concentration of particle-phase species at each step. A single particle wall loss rate constant is in the model as the steady-state size distribution is fairly monodisperse, and is set to 6×10^{-5} s^{-1}.[20] The experimental conditions that were modeled are shown in SI Table 3. The observational data presented here have not been wall-loss corrected because we include particle and vapor wall losses in the model.

The updated F0AM model with gas/particle partitioning and updated isoprene chemistry used in this study can be found at: http://www.atmos.washington.edu/~thornton/washington-aerosol-module.

Quantum Chemical Calculations

To facilitate calculation of the intramolecular RO_2 H-abstraction reactions and subsequent product formation reactions, conformer searches were followed by B3LYP/6-31+G(d) optimizations in Gaussian. For the transition states, constrained optimizations with the same constraints as for the conformer search were conducted before the transition state optimizations. For the subsequent transition state optimizations, the additional optimization keywords "calcfc" and "noeigentest" were used.

Duplicate conformers were removed by a script comparing electronic energies and dipole moments and conformers were marked as identical when their energies were within 10^{-5} H (1 Hatree ≈ 627.5 kcal mol^{-1}) and their dipole moments were within 5×10^{-3} D (1 Debye ≈ 3.33564×10^{-30} Cm). All unique conformers within 2 kcal

mol^{-1} of the lowest energy conformer in electronic energy at the B3LYP/6-31+G(d) level of theory[21, 22] were subsequently optimized using ωB97X-D/aug-cc-pVTZ with the ultrafine integration grid to improve geometries and energies.[23-25] Frequency calculations were carried out to confirm the character of the stationary points identified; no imaginary frequencies for reactant and products and one for transition states corresponding to the motion of the reaction. These frequencies were also used in the zero point vibrational energy correction and in the vibrational partition functions.

For the lowest energy structures of reactant, transition state and product, Molpro 2012.1 was used for single-point calculations on top of the ωB97X-D/aVTZ optimized structures at the ROHF-ROCCSD(T)-F12a/cc-pVDZ-F12 level (abbreviated F12) for more accurate barrier heights.[26-31] In accordance with recommendations, the calculations were carried out using gem beta=0.9, which sets the geminal Slater exponent to 0.9 in the F12 correlation factor.[28]

Reaction rate constants, k, were calculated using multi-conformer transition state theory (MC-TST) including Eckart quantum mechanical tunneling.[32-35]

$$k = \kappa \frac{k_b T}{h} \frac{\sum_i^{All\ TS\ conf.} \exp\left(\frac{-\Delta E_i}{k_B T}\right) Q_{TS,i}}{\sum_j^{All\ R\ conf.} \exp\left(\frac{-\Delta E_j}{k_B T}\right) Q_{R,j}} \exp\left(-\frac{E_{TS,0} - E_{R,0}}{k_B T}\right) \quad \text{(S1)}$$

where κ is the Eckart tunneling coefficient, k_B is the Boltzmann constant, T is the absolute temperature, h is Planck's constant. ΔE_i and ΔE_j are the zero-point corrected energies of conformer i and j of reactant and transition, respectively, relative to the lowest-energy conformer of each, and $Q_{TS,i}$ and $Q_{R,j}$ are the corresponding partition functions. The summations are carried out over all conformers of transition state and reactant, respectively. $E_{TS,0}$ and $E_{R,0}$ are the zero-point corrected energies of the lowest-energy conformer of transition state and reactant, respectively.

In the MC-TST calculation, the F12 energies with ωB97X-D/aug-cc-pVTZ zero-point vibrational corrections were used for the barrier height, while ωB97X-D/aug-cc-pVTZ was used to calculate the relative energy between conformers and partition functions. From the B3LYP/6-31+G(d) geometry of the lowest energy transition state at the ωB97X-D/aug-c-pVTZ level, an IRC was run using B3LYP/6-31+G(d) with the calcall keyword.[36] The end-points were optimized using ωB97X-D/aug-cc-pVTZ and Eckart tunneling was calculated from the ωB97X-D/aug-cc-pVTZ zero-point corrected energies and the imaginary frequency of the transition state at the same level.

Energies and partition functions were corrected using the McClurg approach to hindered rotation as implemented in Gaussian 09 using the "freq= hinderedrotor" keyword.[37-39] The hindered rotor correction to the partition function was divided by the "Multiplicity", which describes the effect from access to different potential energy wells, an effect that is already being accounted for in the MC-TST equation.

Dependence of ISOP(OOH)$_2$ and SOA mass yields on H_2O_2

To understand why the ISOP(OOH)$_2$ and SOA mass yields increase with [H_2O_2] in the chamber and why that is best explained with a competing reaction for the ISOPOOH

derived peroxy radical, we can examine the steady-state relationships for the pertinent molecules, with a focus on $ISOP(OOH)_2$. The production and loss of $ISOP(OOH)_2$, as well as other compounds, can be determined by using the reactions in Table S2. If we assume all components are in steady state, i.e. the production and loss rates are equivalent for each compound, then the steady state concentration of $ISOP(OOH)_2$ can be expressed as shown in equation S2:

$$[ISOP(OOH)_2]_{ss} = \frac{k_{RO_2HO_2}\,[C5H11O6\bullet][HO_2]}{k_1[OH] + k_{h\nu} + k_{dil} + k_{wall}} \quad (S2)$$

where k_1 is the rate constant for the $ISOP(OOH)_2$ and OH reaction and $k_{RO_2HO_2}$ is the MCM default rate constant for RO_2 + HO_2 reactions as discussed previously. The variables k_{hv}, k_{dil}, and k_{wall} refer to the organic peroxide photolysis rate constant, the first-order chamber dilution rate constant (i.e., the inverse chamber residence time), and the vapor wall-loss rate constant, respectively. We neglect gas-particle partitioning in these calculations as we are focusing on the total concentration. We combine $k_{h\nu} + k_{dil} + k_{wall}$ into one k value, hereon denoted as "k_{other}". If we perform the same exercise for the $C_5H_{11}O_6$• peroxy radical, listed as $C_5H_{11}O_6$• in the model, we arrive at:

$$[C_5H_{11}O_6\bullet]_{ss} = \frac{(1-\phi)k_2[ISOPOOH][OH] + k_1[ISOP(OOH)_2][OH]}{k_{isom} + k_{RO_2HO_2}\,[HO_2]} \quad (S3)$$

where 1-ϕ is the yield to the peroxy radical from ISOPOOH + OH as described in Scheme 1 in the main text and k_2 is the rate constant for ISOPOOH + OH. The term $k_1[ISOP(OOH)_2][OH]$ refers to H-abstraction via an OH of the closed-shell $ISOP(OOH)_2$ compound which is a minor source of $C_5H_{11}O_6$• and thus can be set to zero for our purposes here. We ignore k_{dil}, k_{wall}, and k_{cond} for $C_5H_{11}O_6$• as reactions with HO_2 and intra-molecular H-abstraction ("RO_2 isomerization") will dominate. Substituting equation S3 for $C_5H_{11}O_6$• into that for $ISOP(OOH)_2$, equation S2, gives:

$$[ISOP(OOH)_2]_{ss} = \frac{k_{RO_2HO_2}\,[HO_2]\left[\frac{(1-\phi)k_2[ISOPOOH][OH]}{k_{isom} + k_{RO_2HO_2}\,[HO_2]}\right]}{k_1[OH] + k_{other}} \quad (S4)$$

Figure 2 depicts the mass yield of $ISOP(OOH)_2$, i.e. the mass concentration produced relative to the mass concentration of isoprene reacted. The steady state expression for isoprene is:

$$[C_5H_8]_{ss} = \frac{E_{C_5H_8}}{k_3[OH] + k_{dil}} \quad (S5)$$

where $E_{C_5H_8}$ is the emission rate of isoprene into the chamber, held constant, and k_3 is the rate constant for C_5H_8 + OH. The equation for the initial concentration ($[C_5H_8]_i$), i.e. the input concentration is:

$$[C_5H_8]_i = \frac{E_{C_5H_8}}{k_{dil}} \quad \text{(S6)}$$

Thus the steady state expression for the amount of isoprene reacted is:

$$\Delta[C_5H_8]_{ss} = \frac{E_{C_5H_8} k_3[OH]}{{k_{dil}}^2 + k_{dil} k_3[OH]} \quad \text{(S7)}$$

We can substitute the OH concentration at steady state by defining $[OH]_{ss}$ with respect to its two predominant sinks as:

$$[OH]_{ss} = \frac{2k_{h\nu}[H_2O_2]}{k_3[C_5H_8] + k_4[H_2O_2]} \quad \text{(S8)}$$

where k_4 is the rate constant for H_2O_2 + OH and we redefine $k_{h\nu}$ as the photolysis rate constant of H_2O_2. S8 can then be simplified to:

$$[OH]_{ss} = \frac{2k_{h\nu}}{k_4} \quad \text{(S9)}$$

when $k_4[H_2O_2] >> k_3[C_5H_8]$. Using the F0AM model we confirm that the biggest sink of OH is in fact H_2O_2 for a majority of our conditions (Table S3). Thus, $[OH]_{ss}$ is essentially a constant across changing $[H_2O_2]$ in the chamber. Substituting this into equation S7 gives:

$$\Delta[C_5H_8]_{ss} = \frac{E_{C_5H_8} k_3 \frac{2k_{h\nu}}{k_4}}{{k_{dil}}^2 + k_{dil} k_3 \frac{2k_{h\nu}}{k_4}} \quad \text{(S10)}$$

Based on equation S10, the steady-state amount of isoprene reacted is also essentially constant across changing $[H_2O_2]$ until [OH] is of the same order of k_{dil} (Fig. 1, top). We denote S10 from here on as $C_{\Delta I}$. The steady-state mole yield of $ISOP(OOH)_2$ is then the division of equation S4 by S10:

$$\text{Mass yield } ISOP(OOH)_2 = \frac{k_{RO_2HO_2}[HO_2]\left[\frac{(1-\phi)k_2[ISOPOOH][OH]}{k_{isom} + k_{RO_2HO_2}[HO_2]}\right]}{(k_1[OH] + k_{other})\, C_{\Delta I}} \quad \text{(S11)}$$

Given that OH and ϕ are effectively constants, we see from equation S11 that to explain a nearly linear increase in the $ISOP(OOH)_2$ mass yield observed with increasing $[H_2O_2]$ (Fig. 2), changing OH or ϕ are not options (see Fig S4). Even if [OH] changes, it appears in both the numerator and denominator and so the dependence of the $ISOP(OOH)_2$ mass yield on [OH] will be weak. In fact, often $k_1[OH] > k_{other}$, in which case [OH] cancels. Therefore, the explanation must be related to $[HO_2]$ which does increase nearly linearly with H_2O_2 (Fig. S2). It is most instructive to consider the null hypothesis, that k_{isom} is zero, i.e. that intra-molecular H-abstraction of the ISOPOOH derived peroxy radical

does not occur, or occurs much more slowly than reaction with HO_2 ($k_{isom} << k_{RO_2HO_2}[HO_2]$). If that were true, then from equation S11 the dependence of the $ISOP(OOH)_2$ mass yield on $[HO_2]$ would vanish as it is also in the numerator and denominator and there would be no dependence upon $[H_2O_2]$, contrary to what is observed (Fig. 2). Thus, there must be a reaction of the ISOPOOH derived peroxy radical that competes with reaction with HO_2, i.e. a competing reaction that is on the same order as $k_{RO_2HO_2}[HO_2]$. Based on quantum chemical calculations and this analysis, we conclude the competing reaction is intra-molecular H-abstraction ("RO_2 isomerization") followed by O_2 addition. If k_{isom} is on the same order with $k_3[HO_2]$ or larger, then from equation S10 we see that increases in $[HO_2]$ will lead to increases in the $ISOP(OOH)_2$ mass yield in an approximately linear manner, as observed in the measurements. We have shown previously that $ISOP(OOH)_2$ is a major component of the SOA formed under these conditions (suppressed IEPOX multiphase chemistry and high $[H_2O_2]$),[40, 41] and thus is a controlling component of the SOA, including its mass yield. In this way, $[H_2O_2]$ indirectly controls the mass yield of SOA by controlling that of $ISOP(OOH)_2$.

Molecular Formula	**Structure**	**SMILE**	**Abbreviation**
$C_5H_{11}O_6$	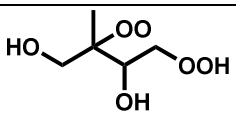	CC(C(O)COO)(O[O])CO	DHHPAO2
$C_5H_{11}O_6$	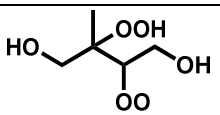	CC(C(O[O])CO)(OO)CO	DHHPBO2
$C_5H_{11}O_6$	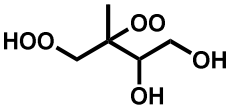	CC(C(O)CO)(O[O])COO	DHHPCO2
$C_5H_{11}O_6$	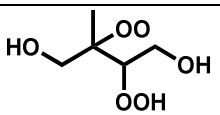	CC(C(OO)CO)(O[O])CO	DHHPDO2
$C_5H_{11}O_7$	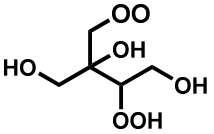	OC(C(OO)CO)(CO[O])CO	THHPO2
$C_5H_{11}NO_7$	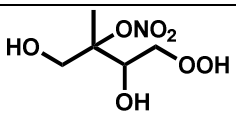	CC(C(O)COO)(O[N+]([O-])=O)CO	DHHPANO3

$C_5H_{11}NO_7$	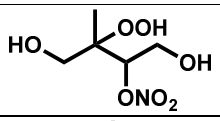	CC(C(O[N+]([O-])=O)CO)(OO)CO	DHHPBNO3
$C_5H_{11}NO_7$	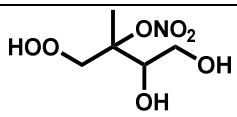	CC(C(O)CO)(O[N+]([O-])=O)COO	DHHPCNO3
$C_5H_{11}NO_7$	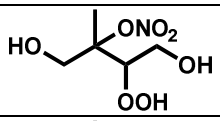	CC(C(OO)CO)(O[N+]([O-])=O)CO	DHHPDNO3
$C_5H_{12}O_6$	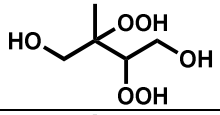	CC(C(OO)CO)(OO)CO	DHDHP
$C_5H_{12}O_5$	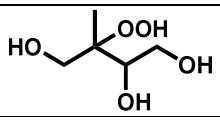	CC(C(O)CO)(OO)CO	THHP
$C_5H_{11}O_5$	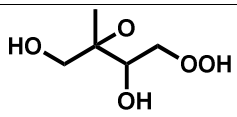	CC(C(O)COO)([O])CO	DHHPAO
$C_5H_{11}O_5$	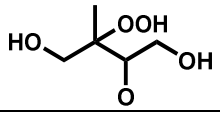	CC(C([O])CO)(OO)CO	DHHPBO
$C_5H_{11}O_5$	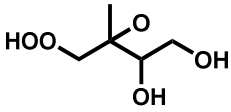	CC(C(O)CO)([O])COO	DHHPCO
$C_5H_{11}O_5$	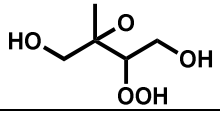	CC(C(OO)CO)([O])CO	DHHPDO
$C_5H_{11}O_6$	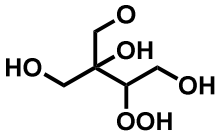	OCC(C(CO)OO)(O)C[O]	THHPO
$C_5H_{11}O_6$	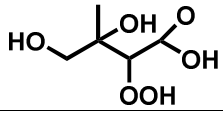	CC(C(C(O)[O])OO)(O)CO	THHPBO
$C_5H_{11}O_4$	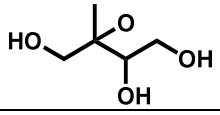	CC([O])(CO)C(O)CO	THBC5O

$C_5H_{11}O_4$	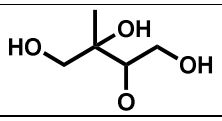	CC(O)(CO)C([O])CO	THACDC5O
$C_5H_{12}O_7$	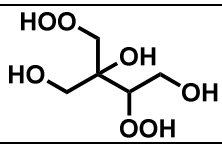	OCC(C(CO)OO)(O)COO	THDHP
$C_5H_{11}NO_8$	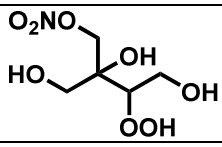	OCC(C(CO)OO)(O)CO[N+]([O-])=O	THHPNO3
$C_5H_{12}O_6$	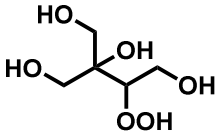	OCC(C(CO)OO)(O)CO	TETROLHP
$C_3H_6O_4$	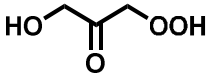	O=C(CO)COO	HYPERACETOL
$C_5H_{10}O_6$	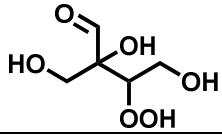	OCC(C(CO)OO)(O)C=O	C5H10O6
$C_5H_{10}O_7$	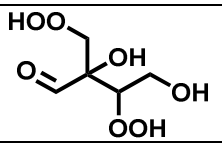	O=CC(C(CO)OO)(O)COO	C5H10O7
$C_5H_{10}O_7$	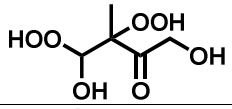	CC(C(CO)=O)(OO)C(OO)O	DHDHPket
$C_5H_{10}O_6$	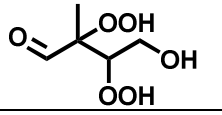	CC(C(CO)OO)(OO)C=O	HDHPald
$C_5H_{10}O_5$	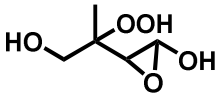	CC(C(O1)C1O)(OO)CO	DHHEPOX
$C_5H_{11}O_5$	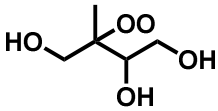	CC(C(CO)O)(O[O])CO	THHO2
$C_5H_{12}O_4$	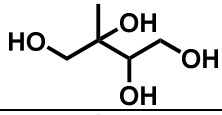	CC(C(CO)O)(O)CO	TETROL
$C_5H_{11}NO_6$	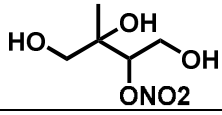	CC(C(CO)O[N+]([O-])=O)(O)CO	THHNO3

$C_5H_{11}O_4$	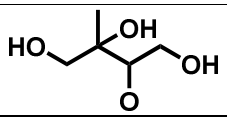	CC(C(CO)[O])(O)CO	THHO
$C_5H_8O_4$	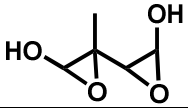	CC(C(O1)C1O)(O2)C2O	C5H8O4epox
$C_5H_8O_5$	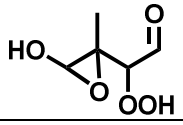	CC(C(OO)C=O)(O1)C1O	C5H8O5
$C_5H_8O_4$	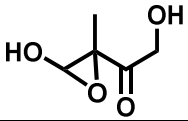	CC(C(CO)=O)(O1)C1O	C5H8O4ald
$C_5H_8O_6$	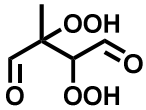	CC(C(C=O)OO)(OO)C=O	DHPDA
$C_5H_8O_5$	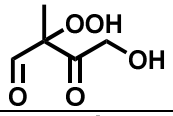	CC(C(CO)=O)(OO)C=O	HHPDc
$C_5H_8O_6$	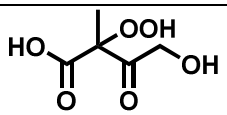	CC(C(CO)=O)(OO)C(O)=O	HHPcarb
$C_5H_8O_7$	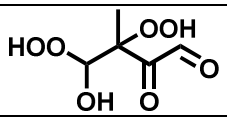	CC(C(C=O)=O)(OO)C(OO)O	HDHPDc

Table S1. The molecular formulas, structures, SMILE, and compound name for each of the compounds added to the base MCM mechanism.

Reaction	**Rate constants (cm^3 $molec^{-1}$ s^{-1})**	**Product Yield**
OH + ISOPAOH = HC4ACHO + HO2	9.3×10^{-11}	0.05
OH + ISOPAOH = HC4CCHO + HO2	9.3×10^{-11}	0.05
OH + ISOPAOH = THHO2	9.3×10^{-11}	0.9
OH + ISOPBOH = MVK + HCHO + HO2	3.85×10^{-11}	0.1
OH + ISOPBOH = THHO2	3.85×10^{-11}	0.9
OH + ISOPDOH = HCOC5 + HO2	7.38×10^{-11}	0.1
OH + ISOPDOH = THHO2	7.38×10^{-11}	0.9
NO3 + ISOPAOOH = IEPOXA + OH	3.15×10^{-12}*exp(-450/T)	1
NO3 + ISOPBOOH = IEPOXB + OH	3.15×10^{-12}*exp(-450/T)	1
NO3 + ISOPCOOH = IEPOXC + OH	3.15×10^{-12}*exp(-450/T)	1
NO3 + ISOPDOOH = IEPOXB + OH	3.15×10^{-12}*exp(-450/T)	1

OH + ISOPAOOH = IEPOXA + OH	1.54×10^{-10}	0.58
OH + ISOPBOOH = IEPOXB + OH	5×10^{-11}	0.7
OH + ISOPCOOH = IEPOXC + OH	1.54×10^{-10}	0.59
OH + ISOPDOOH = IEPOXB + OH	1.15×10^{-10}	0.72
OH + ISOPAOOH = DHHPAO2	1.54×10^{-10}	0.38
OH + ISOPBOOH = DHHPBO2	5×10^{-11}	0.2
OH + ISOPCOOH = DHHPCO2	$1.\ 54\times10^{-10}$	0.39
OH + ISOPDOOH = DHHPDO2	1.15×10^{-10}	0.2
OH + ISOPAOOH = ISOPAO2	1.54×10^{-10}	0.02
OH + ISOPBOOH = ISOPBO2	5×10^{-11}	0.08
OH + ISOPCOOH = ISOPCO2	$1.\ 54\times10^{-10}$	0.02
OH + ISOPDOOH = ISOPDO2	1.15×10^{-10}	0.03
OH + ISOPAOOH = HC4ACHO + OH	1.54×10^{-10}	0.02
OH + ISOPCOOH = HC4CCHO + OH	1.54×10^{-10}	0.02
OH + ISOPDOOH = HCOC5 + OH	1.15×10^{-10}	0.05
THHO2 + Isomerization = C57OOH	0.002	1
THHO2 + NO = THHO + NO2	KRO2NO	0.892
THHO2 + NO = THHNO3	KRO2NO	0.108
THHO2 + NO3 = THHO + NO2	KRO2NO3	1
THHO2 + HO2 = THHP	KRO2HO2	1
THHO2 + RO2 = THHO	2.40×10^{-11}	0.1
THHO2 + RO2 = C58OH	2.40×10^{-11}	0.1
THHO2 + RO2 = TETROL	2.40×10^{-11}	0.8
THHO = THHO2	KDEC	0.25
THHO = TETROL + HO2	KDEC	0.4
THHO = MACROH + HCHO + HO2	KDEC	0.1
THHO = ACETOL + HOCH2CHO + OH	KDEC	0.25
DHHPBO2 + Isomerization = HDHPald	0-0.8	0.0099
DHHPBO2 + Isomerization = DHDHPket	0-0.8	0.0001
DHHPBO2 + Isomerization = DHHEPOX	0-0.8	0.99
DHHPBO2 + NO = DHHPBO + NO2	KRO2NO	0.892
DHHPBO2 + NO = DHHPBNO3	KRO2NO	0.108
DHHPBO2 + NO3 = DHHPBO + NO2	KRO2NO3	1
DHHPBO2 + HO2 = DHDHP	KRO2HO2	1
DHHPBO2 + RO2 = DHHPBO	2.40×10^{-11}	0.1
DHHPBO2 + RO2 = C59OOH	2.40×10^{-11}	0.1
DHHPBO2 + RO2 = THHP	2.40×10^{-11}	0.8
DHHPBO = THHPO2	KDEC	0.25
DHHPBO = C57OOH + HO2	KDEC	0.4
DHHPBO = MACROOH + HCHO + HO2	KDEC	0.1
DHHPBO = ACETOL + HOCH2CHO + OH	KDEC	0.25
DHHPAO2 + Isomerization = HDHPald	0-0.8	0.0099
DHHPAO2 + Isomerization = DHDHPket	0-0.8	0.0001
DHHPAO2 + Isomerization = DHHEPOX	0-0.8	0.99
DHHPAO2 + NO = DHHPAO + NO2	KRO2NO	0.892
DHHPAO2 + NO = DHHPANO3	KRO2NO	0.108

DHHPAO2 + NO3 = DHHPAO + NO2	KRO2NO3	1
DHHPAO2 + HO2 = DHDHP	KRO2HO2	1
DHHPAO2 + RO2 = DHHPAO	2.40×10^{-11}	0.2
DHHPAO2 + RO2 = THHP	2.40×10^{-11}	0.8
DHHPAO = C57OH + OH	KDEC	0.2
DHHPAO = HMVKAOOH + HCHO + HO2	KDEC	0.3
DHHPAO = ACETOL + HCOCH2OOH + HO2	KDEC	0.5
DHHPCO2 + Isomerization = HDHPald	0-0.8	0.0099
DHHPCO2 + Isomerization = DHDHPket	0-0.8	0.0001
DHHPCO2 + Isomerization = DHHEPOX	0-0.8	0.99
DHHPCO2 + NO = DHHPCO + NO2	KRO2NO	0.892
DHHPCO2 + NO = DHHPCNO3	KRO2NO	0.108
DHHPCO2 + NO3 = DHHPCO + NO2	KRO2NO3	1
DHHPCO2 + HO2 = DHDHP	KRO2HO2	1
DHHPCO2 + RO2 = DHHPCO	2.40×10^{-11}	0.2
DHHPCO2 + RO2 = THHP	2.40×10^{-11}	0.8
DHHPCO = C58OOH + HO2	KDEC	0.2
DHHPCO = HO12CO3C4 + HCHO + OH	KDEC	0.3
DHHPCO = HYPERACET + HOCH2CHO + HO2	KDEC	0.5
DHHPCO2 + Isomerization = HDHPald	0-0.8	0.0099
DHHPCO2 + Isomerization = DHDHPket	0-0.8	0.0001
DHHPDO2 + Isomerization = DHHEPOX	0-0.8	0.99
DHHPDO2 + NO = DHHPCO + NO2	KRO2NO	0.892
DHHPDO2 + NO = DHHPCNO3	KRO2NO	0.108
DHHPDO2 + NO3 = DHHPDO + NO2	KRO2NO3	1
DHHPDO2 + HO2 = DHDHP	KRO2HO2	1
DHHPDO2 + RO2 = DHHPDO	2.40×10^{-11}	0.2
DHHPDO2 + RO2 = THHP	2.40×10^{-11}	0.8
DHHPDO = C57OOH + HO2	KDEC	0.5
DHHPDO = HMVKBOOH + HCHO + OH	KDEC	0.25
DHHPDO = ACETOL + HOCH2CHO + HO2	KDEC	0.25
THHPO2 = C5H10O7 + HO2	0	0
THHPO2 + NO = THHPO + NO2	KRO2NO	0.892
THHPO2 + NO = THHPNO3	KRO2NO	0.108
THHPO2 + NO3 = THHPO + NO2	KRO2NO3	0.25
THHPO2 + HO2 = THDHP	KRO2HO2	1
THHPO2 = THHPO	2.40×10^{-12}	0.8
THHPO2 + RO2 = C5H10O6	2.40×10^{-12}	0.1
THHPO2 + RO2 = TETROLHP	2.40×10^{-12}	0.1
THHPO = C5H10O6 + HO2	KDEC	0.1
THHPO = MVKOHAOH + HCHO + OH	KDEC	0.1
THHPO = HO12CO3C4 + HCHO + OH	KDEC	0.25
DHDHP + OH = C58OOH + OH	5×10^{-11}	0.64
DHDHP + OH = DHHPBO2	5×10^{-11}	0.2
DHDHP + OH = DHHPDO2	5×10^{-11}	0.08
DHDHP + OH = DHHPAO2	5×10^{-11}	0.04

DHDHP + OH = DHHPCO2	5×10^{-11}	0.04
THDHP + OH = C5H10O7 + HO2	0	0
THDHP + OH = C5H10O7 + OH	0	0
THDHP + OH = THHPO2	0	0
DHDHP + hv = DHHPBO + OH	J41	0.5
DHDHP + hv = DHHPDO + OH	J41	0.25
DHDHP + hv = DHHPAO + OH	J41	0.125
DHDHP + hv = DHHPCO + OH	J41	0.125
THHP + OH = C57OOH + HO2	5×10^{-11}	0.55
THHP + OH = C58OOH + HO2	5×10^{-11}	0.133
THHP + OH = C57OH + OH	5×10^{-11}	0.067
THHP + OH = THHPO2	5×10^{-11}	0.25
THHP + hv = THBC5O + OH	J41	0.5
THHP + hv = THACDC5O + OH	J41	0.5
THBC5O = C57OH + HO2	KDEC	0.25
THBC5O = HO12CO3C4 + HCHO + HO2	KDEC	0.25
THBC5O = ACETOL + HOCH2CHO + HO2	KDEC	0.5
THACDC5O = MACROH + HCHO + HO2	KDEC	1
THDHP + hv = THHPO + OH	J41	0.5
THDHP + hv = THHPBO + OH	J41	0.5
THHPBO = MVKOHAOH + HCHO + OH	KDEC	0.25
THHPBO = HOCH2CHO + HYPERACETOL + HO2	KDEC	0.25
THHPBO = C5H10O6 + HO2	KDEC	0.25
THHPBO = HMVKBOOH + HCHO + HO2	KDEC	0.25
HYPERACETOL + hv = 2HCHO + HO2 + OH	J41	0.5
HYPERACETOL + hv = HOCH2COCHO +HO2 +OH	J41	0.5
HYPERACETOL + OH = HOCH2COCHO + HO2	5×10^{-11}	0.5
HYPERACETOL + OH = ALCOCH2OOH + OH	5×10^{-11}	0.5
DHHEPOX + OH = C5H8O4epox + OH	5×10^{-11}	0.1
DHHEPOX + OH = C5H8O5	5×10^{-11}	0.1
DHHEPOX + OH = C5H8O4ald + OH	5×10^{-11}	0.8
HDHPald + OH = DHPDA + HO2	5×10^{-11}	0.25
HDHPald + OH = HHPDc	5×10^{-11}	0.25
HDHPald + OH = CO + OH + HMVKBOOH	5×10^{-11}	0.5
DHDHPket + OH = HHPcarb + OH	5×10^{-11}	0.5
DHDHPket + OH = HDHPDc + HO2	5×10^{-11}	0.5

Table S2. Complete list of all reactions, rate constants, and yields added to the MCM isoprene mechanism to reflect the $C_5H_{12}O_6$ mechanism, as well as alterations to the MCM as discussed in the text.

Run	Input C_5H_8 (ppbv)	Input H_2O_2 (ppm)	OA ($\mu g\ m^{-3}$)
1	20	10	2.6
2	20	2	1.1
3	20	5	1.8
4	20	0.15	0.2

Table S3. Experimental conditions that were used as input values for the modeling.

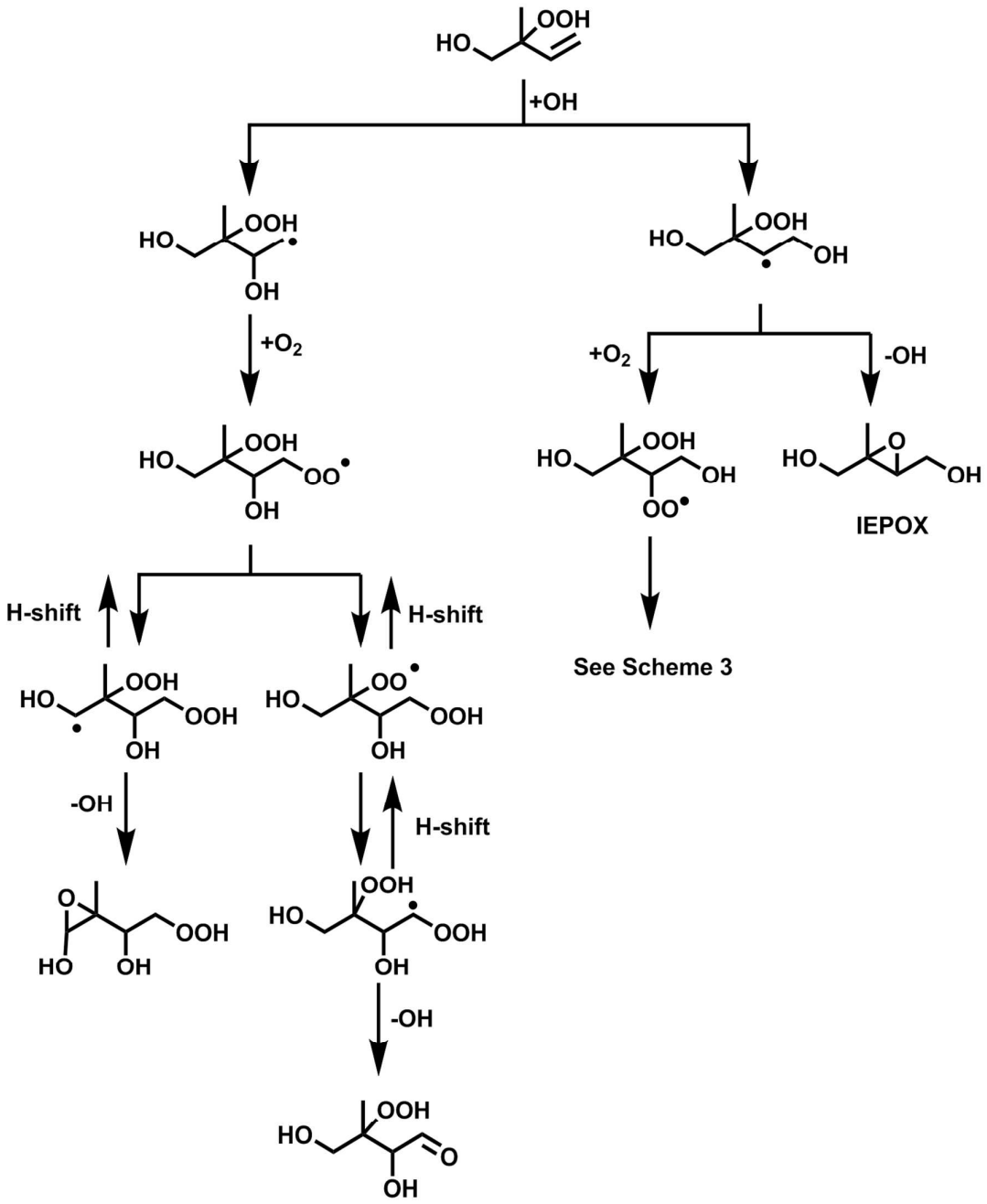

286
287
288 **Scheme S1.** Additional reaction pathway for ISOPOOH + OH to form an additional
289 $C_5H_{10}O_5$ compound.

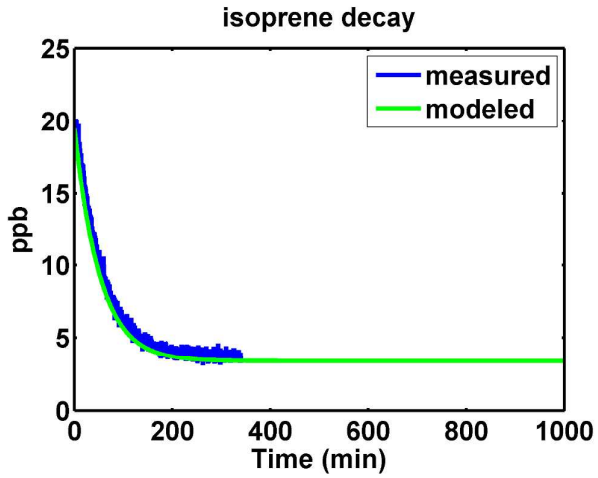

Figure S1. 20 ppb isoprene was introduced into the chamber with lights off, followed by lights on to observe the decay of isoprene. This was used to tune our H_2O_2 photolysis rate.

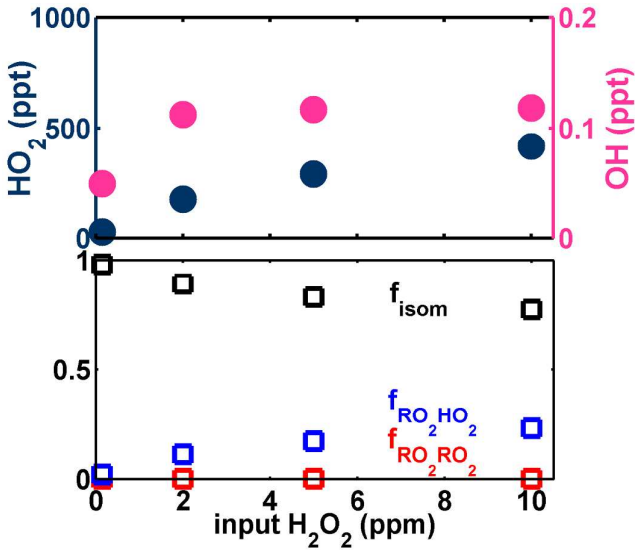

Figure S2. Top: the modeled concentration of HO_2 (ppt, left axis) and OH (ppt, right axis) as a function of input H_2O_2. Bottom: the fraction of $C_5H_{11}O_6$• peroxy radical undergoing isomerization (black) versus reaction with HO_2 (blue) and RO_2 (red).

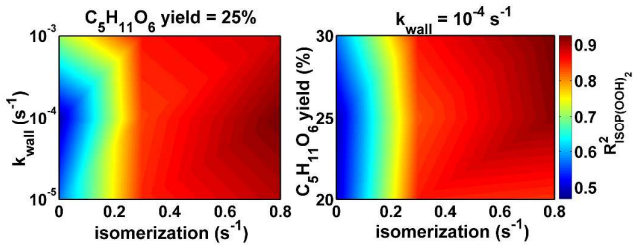

Figure S3. Left: vapor wall loss as a function of isomerization rate at a fixed $C_5H_{11}O_6$• yield of 25%. Right: $C_5H_{11}O_6$• yield versus isomerization rate at a fixed vapor wall loss of 10^{-4} s^{-1}. Both plots are shaded by the R^2 between the measured and modeled $C_5H_{12}O_6$ at the set of conditions.

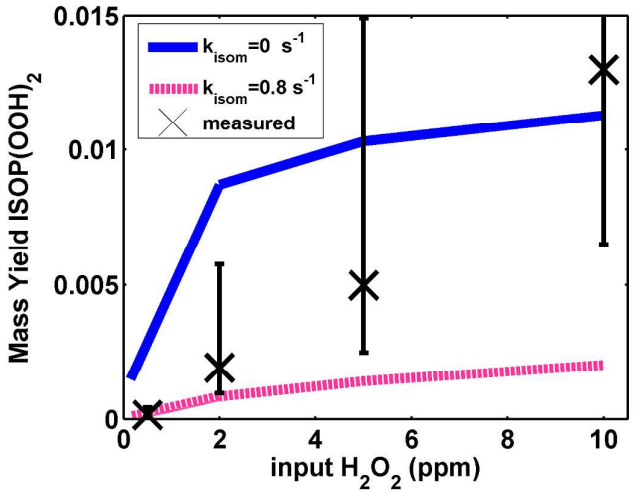

Figure S4. A version of Figure 2 in the main text, redone with model runs with an IEPOX yield of 90% and $C_5H_{11}O_6$• yield of 2%.

References

1. Wolfe, G. M.; Marvin, M. R.; Roberts, S. J.; Travis, K. R.; Liao, J., The Framework for 0-D Atmospheric Modeling (F0AM) v3.1. *Geosci. Model Dev.* **2016,** *9* (9), 3309-3319; doi 10.5194/gmd-9-3309-2016.
2. Wolfe, G. M.; Thornton, J. A., The Chemistry of Atmosphere-Forest Exchange (CAFE) Model - Part 1: Model description and characterization. *Atmos. Chem. Phys.* **2011,** *11* (1), 77-101; doi 10.5194/acp-11-77-2011.
3. Wolfe, G. M.; Thornton, J. A.; Bouvier-Brown, N. C.; Goldstein, A. H.; Park, J. H.; McKay, M.; Matross, D. M.; Mao, J.; Brune, W. H.; LaFranchi, B. W.; Browne, E. C.; Min, K. E.; Wooldridge, P. J.; Cohen, R. C.; Crounse, J. D.; Faloona, I. C.; Gilman, J. B.; Kuster, W. C.; de Gouw, J. A.; Huisman, A.; Keutsch, F. N., The Chemistry of Atmosphere-Forest Exchange (CAFE) Model - Part 2: Application to BEARPEX-2007 observations. *Atmos. Chem. Phys.* **2011,** *11* (3), 1269-1294; doi 10.5194/acp-11-1269-2011.
4. Wolfe, G. M.; Thornton, J. A.; McKay, M.; Goldstein, A. H., Forest-atmosphere exchange of ozone: sensitivity to very reactive biogenic VOC emissions and implications for in-canopy photochemistry. *Atmos. Chem. Phys.* **2011,** *11* (15), 7875-7891; doi 10.5194/acp-11-7875-2011.
5. Jenkin, M. E.; Young, J. C.; Rickard, A. R., The MCM v3.3.1 degradation scheme for isoprene. *Atmos. Chem. Phys.* **2015,** *15* (20), 11433-11459; doi 10.5194/acp-15-11433-2015.
6. Kim, S.; Wolfe, G. M.; Mauldin, L.; Cantrell, C.; Guenther, A.; Karl, T.; Turnipseed, A.; Greenberg, J.; Hall, S. R.; Ullmann, K.; Apel, E.; Hornbrook, R.; Kajii, Y.; Nakashima, Y.; Keutsch, F. N.; DiGangi, J. P.; Henry, S. B.; Kaser, L.; Schnitzhofer, R.; Graus, M.; Hansel, A.; Zheng, W.; Flocke, F. F., Evaluation of HOx sources and cycling using measurement-constrained model calculations in a 2-methyl-3-butene-2-ol (MBO) and monoterpene (MT) dominated ecosystem. *Atmos. Chem. Phys.* **2013,** *13* (4), 2031-2044; doi 10.5194/acp-13-2031-2013.
7. Wolfe, G. M.; Cantrell, C.; Kim, S.; Mauldin, R. L.; Karl, T.; Harley, P.; Turnipseed, A.; Zheng, W.; Flocke, F.; Apel, E. C.; Hornbrook, R. S.; Hall, S. R.; Ullmann, K.; Henry, S. B.; DiGangi, J. P.; Boyle, E. S.; Kaser, L.; Schnitzhofer, R.; Hansel, A.; Graus, M.; Nakashima, Y.; Kajii, Y.; Guenther, A.; Keutsch, F. N., Missing peroxy radical sources within a summertime ponderosa pine forest. *Atmos. Chem. Phys.* **2014,** *14* (9), 4715-4732; doi 10.5194/acp-14-4715-2014.
8. Kim, S.; Kim, S. Y.; Lee, M.; Shim, H.; Wolfe, G. M.; Guenther, A. B.; He, A.; Hong, Y.; Han, J., Impact of isoprene and HONO chemistry on ozone and OVOC formation in a semirural South Korean forest. *Atmos. Chem. Phys.* **2015,** *15* (8), 4357-4371; doi 10.5194/acp-15-4357-2015.
9. Kaiser, J.; Skog, K. M.; Baumann, K.; Bertman, S. B.; Brown, S. B.; Brune, W. H.; Crounse, J. D.; de Gouw, J. A.; Edgerton, E. S.; Feiner, P. A.; Goldstein, A. H.; Koss, A.; Misztal, P. K.; Nguyen, T. B.; Olson, K. F.; St Clair, J. M.; Teng, A. P.; Toma, S.; Wennberg, P. O.; Wild, R. J.; Zhang, L.; Keutsch, F. N., Speciation of OH reactivity

above the canopy of an isoprene-dominated forest. *Atmos. Chem. Phys.* **2016,** *16* (14), 9349-9359; doi 10.5194/acp-16-9349-2016.
10. Feiner, P. A.; Brune, W. H.; Miller, D. O.; Zhang, L.; Cohen, R. C.; Romer, P. S.; Goldstein, A. H.; Keutsch, F. N.; Skog, K. M.; Wennberg, P. O.; Nguyen, T. B.; Teng, A. P.; DeGouw, J.; Koss, A.; Wild, R. J.; Brown, S. S.; Guenther, A.; Edgerton, E.; Baumann, K.; Fry, J. L., Testing Atmospheric Oxidation in an Alabama Forest. *J. Atmos. Sci.* **2016,** *73* (12), 4699-4710; doi 10.1175/jas-d-16-0044.1.
11. Kaiser, J.; Wolfe, G. M.; Bohn, B.; Broch, S.; Fuchs, H.; Ganzeveld, L. N.; Gomm, S.; Haseler, R.; Hofzumahaus, A.; Holland, F.; Jager, J.; Li, X.; Lohse, I.; Lu, K.; Prevot, A. S. H.; Rohrer, F.; Wegener, R.; Wolf, R.; Mentel, T. F.; Kiendler-Scharr, A.; Wahner, A.; Keutsch, F. N., Evidence for an unidentified non-photochemical ground-level source of formaldehyde in the Po Valley with potential implications for ozone production. *Atmos. Chem. Phys.* **2015,** *15* (3), 1289-1298; doi 10.5194/acp-15-1289-2015.
12. Wolfe, G. M.; Hanisco, T. F.; Arkinson, H. L.; Bui, T. P.; Crounse, J. D.; Dean-Day, J.; Goldstein, A.; Guenther, A.; Hall, S. R.; Huey, G.; Jacob, D. J.; Karl, T.; Kim, P. S.; Liu, X.; Marvin, M. R.; Mikoviny, T.; Misztal, P. K.; Nguyen, T. B.; Peischl, J.; Pollack, I.; Ryerson, T.; St Clair, J. M.; Teng, A.; Travis, K. R.; Ullmann, K.; Wennberg, P. O.; Wisthaler, A., Quantifying sources and sinks of reactive gases in the lower atmosphere using airborne flux observations. *Geophys. Res. Lett.* **2015,** *42* (19), 8231-8240; doi 10.1002/2015gl065839.
13. Kaiser, J.; Wolfe, G. M.; Min, K. E.; Brown, S. S.; Miller, C. C.; Jacob, D. J.; deGouw, J. A.; Graus, M.; Hanisco, T. F.; Holloway, J.; Peischl, J.; Pollack, I. B.; Ryerson, T. B.; Warneke, C.; Washenfelder, R. A.; Keutsch, F. N., Reassessing the ratio of glyoxal to formaldehyde as an indicator of hydrocarbon precursor speciation. *Atmos. Chem. Phys.* **2015,** *15* (13), 7571-7583; doi 10.5194/acp-15-7571-2015.
14. Wolfe, G. M.; Kaiser, J.; Hanisco, T. F.; Keutsch, F. N.; de Gouw, J. A.; Gilman, J. B.; Graus, M.; Hatch, C. D.; Holloway, J.; Horowitz, L. W.; Lee, B. H.; Lerner, B. M.; Lopez-Hilifiker, F.; Mao, J.; Marvin, M. R.; Peischl, J.; Pollack, I. B.; Roberts, J. M.; Ryerson, T. B.; Thornton, J. A.; Veres, P. R.; Warneke, C., Formaldehyde production from isoprene oxidation across NOx regimes. *Atmos. Chem. Phys.* **2016,** *16* (4), 2597-2610; doi 10.5194/acp-16-2597-2016.
15. Busilacchio, M.; Di Carlo, P.; Aruffo, E.; Biancofiore, F.; Salisburgo, C. D.; Giammaria, F.; Bauguitte, S.; Lee, J.; Moller, S.; Hopkins, J.; Punjabi, S.; Andrews, S.; Lewis, A. C.; Parrington, M.; Palmer, P. I.; Hyer, E.; Wolfe, G. M., Production of peroxy nitrates in boreal biomass burning plumes over Canada during the BORTAS campaign. *Atmos. Chem. Phys.* **2016,** *16* (5), 3485-3497; doi 10.5194/acp-16-3485-2016.
16. Muller, M.; Anderson, B. E.; Beyersdorf, A. J.; Crawford, J. H.; Diskin, G. S.; Eichler, P.; Fried, A.; Keutsch, F. N.; Mikoviny, T.; Thornhill, K. L.; Walega, J. G.; Weinheimer, A. J.; Yang, M.; Yokelson, R. J.; Wisthaler, A., In situ measurements and

389 modeling of reactive trace gases in a small biomass burning plume. *Atmos. Chem.*
390 *Phys.* **2016,** *16* (6), 3813-3824.
391 17. Riedel, T. P.; Wolfe, G. M.; Danas, K. T.; Gilman, J. B.; Kuster, W. C.; Bon, D. M.;
392 Vlasenko, A.; Li, S. M.; Williams, E. J.; Lerner, B. M.; Veres, P. R.; Roberts, J. M.;
393 Holloway, J. S.; Lefer, B.; Brown, S. S.; Thornton, J. A., An MCM modeling study of
394 nitryl chloride (ClNO2) impacts on oxidation, ozone production and nitrogen oxide
395 partitioning in polluted continental outflow. *Atmos. Chem. Phys.* **2014,** *14* (8), 3789-
396 3800; doi 10.5194/acp-14-3789-2014.
397 18. Wolfe, G. M.; Crounse, J. D.; Parrish, J. D.; St. Clair, J. M.; Beaver, M. R.; Paulot,
398 F.; Yoon, T. P.; Wennberg, P. O.; Keutsch, F. N., Photolysis, OH reactivity and ozone
399 reactivity of a proxy for isoprene-derived hydroperoxyenals (HPALDs). *Phys. Chem.*
400 *Chem. Phys.* **2012,** *14* (20), 7276-7286; doi 10.1039/c2cp40388a.
401 19. Kaiser, J.; Li, X.; Tillmann, R.; Acir, I.; Holland, F.; Rohrer, F.; Wegener, R.;
402 Keutsch, F. N., Intercomparison of Hantzsch and fiber-laser-induced-fluorescence
403 formaldehyde measurements. *Atmos. Meas. Tech.* **2014,** *7* (6), 1571-1580; doi
404 10.5194/amt-7-1571-2014.
405 20. Crump, J. G.; Flagan, R. C.; Seinfeld, J. H., Particle wall loss rates in vessels.
406 *Aerosol Sci. Technol.* **1983,** *2* (3), 303-309; doi 10.1080/02786828308958636.
407 21. Kurten, T.; Rissanen, M. P.; Mackeprang, K.; Thornton, J. A.; Hyttinen, N.;
408 Jørgensen, S.; Ehn, M.; Kjaergaard, H. G., Computational study of hydrogen shifts
409 and ring-opening mechanisms in alpha-pinene ozonolysis products. *J. Phys. Chem. A*
410 **2015,** *119* (46), 11366-11375; doi 10.1021/acs.jpca.5b08948.
411 22. Rissanen, M. P.; Kurten, T.; Sipila, M.; Thornton, J. A.; Kangasluoma, J.;
412 Sarnela, N.; Junninen, H.; Jørgensen, S.; Schallhart, S.; Kajos, M. K.; Taipale, R.;
413 Springer, M.; Mentel, T. F.; Ruuskanen, T.; Petaja, T.; Worsnop, D. R.; Kjaergaard, H.
414 G.; Ehn, M., The formation of highly oxidized multifunctional products in the
415 ozonolysis of cyclohexene. *J. Am. Chem. Soc.* **2014,** *136* (44), 15596-15606; doi
416 10.1021/ja507146s.
417 23. Chai, J.-D.; Head-Gordon, M., Long-range corrected hybrid density
418 functionals with damped atom-atom dispersion corrections. *Phys. Chem. Chem.*
419 *Phys.* **2008,** *10* (44), 6615-6620; doi 10.1039/b810189b.
420 24. Dunning, T. H., Gaussian-basis sets for use in correlated molecular
421 calculations .1. The atoms boron through neon and hydrogen. *J. Chem. Phys.* **1989,**
422 *90* (2), 1007-1023; doi 10.1063/1.456153.
423 25. Kendall, R. A.; Dunning, T. H.; Harrison, R. J., Electron-affinities of the 1st-
424 row atoms revisted- Systematic basis-sets and wave-functions *J. Chem. Phys.* **1992,**
425 *96* (9), 6796-6806; doi 10.1063/1.462569.
426 26. Adler, T. B.; Knizia, G.; Werner, H. J., A simple and efficient CCSD(T)-F12
427 approximation. *J. Chem. Phys.* **2007,** *127* (22), doi 10.1063/1.2817618.
428 27. Knizia, G.; Adler, T. B.; Werner, H. J., Simplified CCSD(T)-F12 methods:
429 Theory and benchmarks. *J. Chem. Phys.* **2009,** *130* (5), doi 10.1063/1.3054300.

28. Peterson, K. A.; Adler, T. B.; Werner, H. J., Systematically convergent basis sets for explicitly correlated wavefunctions: The atoms H, He, B-Ne, and Al-Ar. *J. Chem. Phys.* **2008,** *128* (8), doi 10.1063/1.2831537.
29. Werner, H. J.; Knizia, G.; Manby, F. R., Explicitly correlated coupled cluster methods with pair-specific geminals. *Mol. Phys.* **2011,** *109* (3), 407-417; doi 10.1080/00268976.2010.526641.
30. Werner, H. J.; Knowles, P. J.; Knizia, G.; Manby, F. R.; Schütz, M.; Celani, P.; Györffy, W.; Kats, D.; Korona, T.; Lindh, R.; Mitrushenkov, A.; Rauhut, G.; Shamasundar, K. R.; Adler, T. B.; Amos, R. D.; Bernhardsson, A.; Berning, A.; Cooper, D. L.; Deegan, M. J. O.; Dobbyn, A. J.; Eckert, F.; Goll, E.; Hampel, C.; Hesselmann, A.; Hetzer, G.; Hrenar, T.; Jansen, G.; Köppl, C.; Liu, Y.; Lloyd, A. W.; Mata, R. A.; May, A. J.; McNicholas, S. J.; Meyer, W.; Mura, M. E.; Nicklass, A.; O'Neill, D. P.; Palmieri, P.; Peng, D.; Pflüger, K.; Pitzer, R.; Reiher, M.; Shiozaki, T.; Stoll, H.; Stone, A. J.; Tarroni, R.; Thorsteinsson, T.; Wang, M., Molpro, version 2012.1, a package of ab initio programs. **2012**.
31. Watts, J. D.; Gauss, J.; Bartlett, R. J., Coupled-cluster methods with noniterative triple excitations for restricted open-shell Hartree-Fock and other general single determinant reference functions - Energies and analytical gradients *J. Chem. Phys.* **1993,** *98* (11), 8718-8733; doi 10.1063/1.464480.
32. Eckart, C., The penetration of a potential barrier by electrons. *Phys. Rev.* **1930,** *35* (11), 1303-1309; doi 10.1103/PhysRev.35.1303.
33. Eyring, H., The activated complex in chemical reactions. *J. Chem. Phys.* **1935,** *3* (2), 107-115; doi 10.1063/1.1749604.
34. Møller, K. H.; Otkjær, R. V.; Hyttinen, N.; Kurtén, T.; Kjaergaard, H. G., Cost-Effective Implementation of Multiconformer Transition State Theory for Peroxy Radical Hydrogen Shift Reactions. *J. Phys. Chem. A* **2016,** *120* (51), 10072-10087; doi 10.1021/acs.jpca.6b09370.
35. Vereecken, L.; Peeters, J., The 1,5-H-shift in 1-butoxy: A case study in the rigorous implementation of transition state theory for a multirotamer system. *J. Chem. Phys.* **2003,** *119* (10), 5159-5170; doi 10.1063/1.1597479.
36. Fukui, K., The path of chemical-reactions - The IRC approach *Accounts Chem. Res.* **1981,** *14* (12), 363-368; doi 10.1021/ar00072a001.
37. Ayala, P. Y.; Schlegel, H. B., Identification and treatment of internal rotation in normal mode vibrational analysis. *J. Chem. Phys.* **1998,** *108* (6), 2314-2325; doi 10.1063/1.475616.
38. McClurg, R. B., Comment on "The hindered rotor density-of-states interpolation function" J. Chem. Phys. 106, 6675 (1997) and "The hindered rotor density-of-states" J. Chem. Phys. 108, 2314 (1998). *J. Chem. Phys.* **1999,** *111* (15), 7163-7164; doi 10.1063/1.480272.
39. McClurg, R. B.; Flagan, R. C.; Goddard, W. A., The hindered rotor density-of-states interpolation function. *J. Chem. Phys.* **1997,** *106* (16), 6675-6680; doi 10.1063/1.473664.

40. D'Ambro, E. L.; Lee, B. H.; Liu, J.; Shilling, J. E.; Gaston, C. J.; Lopez-Hilfiker, F. D.; Schobesberger, S.; Zaveri, R. A.; Mohr, C.; Lutz, A.; Zhang, Z.; Gold, A.; Surratt, J. D.; Rivera-Rios, J. C.; Keutsch, F. N.; Thornton, J. A., Molecular composition and volatility of isoprene photochemical oxidation secondary organic aerosol under low- and high-NOx conditions. *Atmos. Chem. Phys.* **2017,** *17* (1), 159-174; doi 10.5194/acp-17-159-2017.

41. Liu, J. M.; D'Ambro, E. L.; Lee, B. H.; Lopez-Hilfiker, F. D.; Zaveri, R. A.; Rivera-Rios, J. C.; Keutsch, F. N.; Iyer, S.; Kurten, T.; Zhang, Z. F.; Gold, A.; Surratt, J. D.; Shilling, J. E.; Thornton, J. A., Efficient isoprene secondary organic aerosol formation from a non-IEPOX pathway. *Environ. Sci. Technol.* **2016,** *50* (18), 9872-9880; doi 10.1021/acs.est.6b01872.